

Wave aberrations of the isolated crystalline lens

Austin Roorda

University of Houston College of Optometry, Houston, TX, USA



Adrian Glasser

University of Houston College of Optometry, Houston, TX, USA



A method to measure wave aberrations in the isolated crystalline lens is demonstrated. The method employs a laser scanning technique in which the trajectories of narrow refracted laser beams are measured for an array of sample positions incident on the lens. The local slope of the emerging wavefront is calculated for each sample position, and a least squares procedure is used to fit a Zernike polynomial function to define the wave aberration. Measurements of the aberrations of an isolated porcine lens and macaque lens undergoing changes in accommodative state with mechanical stretching are shown. Many aberrations were present, but negative spherical aberration dominated. In the macaque lens, many aberrations underwent systematic changes with accommodation, most notably the 4th order spherical aberration, which became more negative, and the 6th order spherical aberration, which progressed from negative to positive.

Keywords: aberrations, lens, accommodation

Introduction

Laser ray trace scanning technique

Laser ray-tracing optical measurements have been used previously to measure optical properties of isolated crystalline lenses from many species to understand gradient refractive index distribution, monochromatic aberrations, chromatic aberrations, development, aging, and accommodation (Campbell & Hughes, 1981; Sivak, 1982; Sivak & Dovrat, 1983; Sivak & Kreuzer, 1983; Campbell, 1984; Kreuzer & Sivak, 1985; Dovrat, Sivak, & Gershon, 1986; Chan, Ennis, Pierscionek, & Smith, 1988; Axelrod, Lerner, & Sands, 1988; Pierscionek, Chan, Ennis, Smith, & Augusteyn, 1988; Kröger, Campbell, Munger, & Fernald, 1994; Glasser & Howland, 1995; Glasser & Campbell, 1998; Glasser & Campbell, 1999; Kröger, Campbell, & Fernald, 2001).

In situ, the crystalline lens exists in an aqueous environment, bathed on the anterior surface by the aqueous and on the posterior surface by the vitreous. A precise understanding of the optical properties and function of the crystalline lens requires an understanding of the lens optical properties in an aqueous environment of appropriate refractive index. Crystalline lens optical properties, such as focal length and spherical aberration, can be measured by utilizing the optical power of the lens to refract fine parallel incident collimated laser beams in a physiological saline solution of refractive index approximating that of the aqueous and vitreous in the eye. Tracing the path of parallel laser beams as they are refracted by the lens and reconstructing these paths provide a means to study the lens optical properties and function. Such measurements can be made by taking a single photograph of a fan of parallel rays simultaneously incident on a lens or by digitizing the path

of a single ray in a stepwise manner as the laser beam is scanned horizontally or vertically across the face of the lens. The optical axis is determined by the ray that passes undeviated through the lens, and the focal length is determined from the mean intersection point of each ray with the optical axis. Spherical aberration can be determined from the difference in dioptric distance of peripheral refracted rays incident at the edge of the lens and paraxial refracted rays incident near the optical axis of the lens (Glasser & Campbell, 1998; Glasser & Campbell, 1999). Astigmatism can be measured by considering the difference in focal length of scans at orthogonal meridians across the lens. Efforts have also been made to use laser ray-tracing techniques to understand the gradient refractive index of the lens by consideration of the laser ray path through the lens, the entry point of parallel rays incident on the lens and the exit point of refracted rays leaving the lens (Axelrod et al., 1988). However, no previous attempts have been made to characterize the wave aberrations of crystalline lenses from direct measurements.

Sources of aberrations in the eye

Recent evidence suggests that the lens has a role in compensating for spherical aberration of the cornea, as a means to reduce the aberrations of the whole eye (Artal, Guirao, Berrio, & Williams, 2001; Artal, Berrio, Guirao, & Piers, 2002), although prior studies suggested that no such compensation exists (Millodot & Sivak, 1979; Sivak, 1982; Sivak & Kreuzer, 1983). Indirect methods to estimate lenticular aberrations in living eyes consider measuring the whole eye aberrations and subtracting the aberrations of the front surface of the cornea (Artal et al., 2001; Artal & Guirao, 1998), which can give rise to erroneous results if the axes are not properly controlled between the two measurements (Salmon & Thibos, 2002). Alternately, one can measure the aberrations of the eye after eliminating the

power of the cornea (Artal et al., 2001). In either method, the aberrations of the lens are confounded with the aberrations of the posterior surface of the cornea (Guirao & Artal, 2000; Barbero, Marcos, & Merayo-Lloves, 2002). Assessment of lens aberrations by direct measurements on isolated lenses is not subject to the same problems. On the other hand, measurements of the isolated lens cannot address the corneal-lenticular compensation, because nothing is known about the specific corneal aberrations, nor of the influence of the aberrations due to nonparallel, convergent incident rays striking the lens when the cornea is present. The alignments of the cornea, lens, and pupil are also important factors that cannot be addressed. Nonetheless, the optical properties of the *isolated* crystalline lens are essential to implicate the actual sources of the compensation.

Dynamic changes in the lens

Changes in the wave aberrations of the crystalline lens due to accommodation are important to understand, especially as they relate to image quality at different viewing distances and the mechanism of accommodation in the eye. A host of studies of the wave aberration of the whole eye have shown that aberrations change with accommodation (Jenkins, 1963; Koomen, Tousey, & Scolnik, 1949; Ivanoff, 1956; Atchison, Collins, Wildsoet, Christensen, & Waterworth, 1995; Lu, Campbell, & Munger, 1994; He & Marcos, 2000). Three main results have been found. First, it is suggested that the magnitude of the aberrations change with accommodation in such a way that they reach a minimum at an intermediate level of accommodation. The typical level of accommodation for minimum aberrations was found to be about 2 D, or a 50-cm viewing distance (He & Marcos, 2000). Second, the spherical aberration of the eye tends toward a more negative state as the eye accommodates (Jenkins, 1963; Hofer, Artal, Aragon, & Williams, 2001) (Cheng, Barnett, Vilupuru, Marsack, Kasthurirangan, Applegate, & Roorda, 2004). Measurements along a single meridian of the isolated human crystalline lens undergoing accommodative changes with mechanical stretching have revealed the same trend (Glasser & Campbell, 1999). Finally, the change in aberrations with accommodation is of a similar magnitude as the aberration itself (Williams, Yoon, Guirao, Hofer, & Porter, 2001). These changes in aberrations that occur with accommodation must be dominated by changes in the lens. It is unknown if the changes in aberrations that occur as the eye accommodates are functionally important for vision, or are simply a byproduct of the change in power of the lens. A recent study in monkeys suggests that changes in aberrations serve to accentuate the accommodative changes (Vilupuru, Roorda, & Glasser, 2004). Ocular accommodative aberrations changes limit the benefit of treatments aimed at correcting aberrations of the eye through laser ablation. Understanding the accommodative changes in aberrations of the lens may help to understand how the crystalline lens accommo-

dates, and may also aid in the design of fixed, or accommodating intraocular lens implants.

In vitro lens studies

In vitro studies on the isolated lens allow the entire lens to be measured, not just the zone that is accessible through the pupil in the living eye. Whereas the pupil defines the region that is important for vision, examining the entire lens is useful for learning about its overall changes and can be used to better understand the underlying mechanisms that govern lens optical properties and performance.

Methods

Scanning laser apparatus

The scanning laser optical performance evaluator (SLOPE) is shown in Figure 1. This instrument was developed from experience with similar instruments that allowed measurements in only one meridian (Glasser & Campbell, 1998; Glasser & Campbell, 1999). A 633-nm wavelength HeNe laser beam is reflected off two front-surfaced mirrors mounted on stepper motor stages (MotionMaster 3000, Newport Corp.). The stages are orthogonal to each other to provide motion in an *x* (horizontal) and *y* (vertical) direction. After reflection from the second mirror, the horizontally directed laser beam enters a glass chamber filled with saline. A small quantity of powdered milk in the saline allows the laser beam to be visualized in the solution. A crystalline lens is positioned in the solution in the path of the laser beam either by placing the isolated (pig) lens on a molded putty pedestal or by attaching the partially dissected anterior segment of an eye (rhesus monkey) to a mechanical stretching apparatus (see below). Two CCD video cameras positioned above and to the side of the glass chamber allow the laser beam entering (entrance beam) and exiting the crystalline lens (exit beam) to be imaged simultaneously. The video images are captured by a video capture card (ICPCI, AM-VS, Imaging Technology Inc.) in a personal computer. A macro written for Optimas Image Analysis software (Media Cybernetics) moves the *x*- and *y*-translation stages to position the entrance laser beam on the lens. Movement of the stages to a predetermined sequence of positions delivers a specified laser spot pattern onto the anterior surface of the lens. The paths of the laser beams in the solution are digitized, and the slopes and intercepts of the entrance and exit beams are calculated. An alignment procedure ensures that image magnification is identical, that the horizontal and vertical cameras view the same image field, and that the laser beam is passing through the optical axis of the lens (no deviation between entrance and exit beams) in the *x* and *y* planes. Minor physiological asymmetries in the lenses limit the precision with which the alignment can be achieved, preventing, for example, alignment of the lens such that the anterior surface is nor-

mal to the optical axis laser beam. The scanning procedure moves the stages to position the laser sequentially at each x , y position of the pre-specified spot pattern. At each laser beam position, the laser entrance and exit beams are digitized three times, and the slopes and intercepts of each beam are recorded each time and saved to a file together with the location of the x , y stepper motor positions. The data from the three iterations at each laser beam position are averaged to reconstruct the three dimensional trajectory of each laser beam entering and exiting the crystalline lens. The intersection point of the entrance and exit beam is calculated for each laser beam position to determine the principal plane of the lens. The position in the x and y planes where each exit beam crosses the optical axis is also determined. The mean focal plane of the lens is determined as the average position of intersection of each exit beam with the optical axis. The transverse deviation of each exit beam from the optical axis at the focal plane is calculated. The mean focal length of the lens, the transverse deviation, and the x and y stepper motor positions are saved to a file for subsequent analysis.

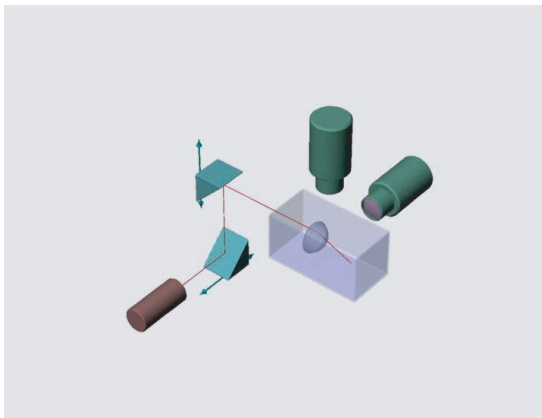


Figure 1. Scanning laser optical performance evaluator (SLOPE). The system consists of a laser, two mirrors mounted on translation stages, a chamber filled with saline in which the lens is placed, and two CCD cameras, one above and the other to the side of the glass chamber. The cameras view the trajectory of the laser beams as they enter and are refracted by the crystalline lens.

Mechanical stretching apparatus

The eye is dissected by removing the cornea and anterior sclera, cutting through the uvea posterior of the ora serrata to isolate the anterior segment tissue comprising the anterior ciliary body and the lens still naturally suspended by the zonular fibers. The vitreous is completely removed from the posterior lens surface by aspiration and cutting with scissors without damaging the lens. Mechanical stretching is done with a dilator (Figure 2), which is similar to that described previously (Glasser & Campbell, 1998). The mechanism of action is similar to that of a scroll chuck dilator. The dilator ring has 12 radially oriented arms. Pins

extending from each arm insert into spiral grooves in a circular base plate. When the base plate is rotated, the stretching arms move inward or outward in unison (see movie in Figure 2b). The tips of the arms are glued to the anterior ciliary body of the dissected eye with cyanoacrylate Super Glue in the same manner as described previously (Glasser & Campbell, 1998) (Figure 2). The lens is always scanned with the anterior surface forward. Although superior, infe-

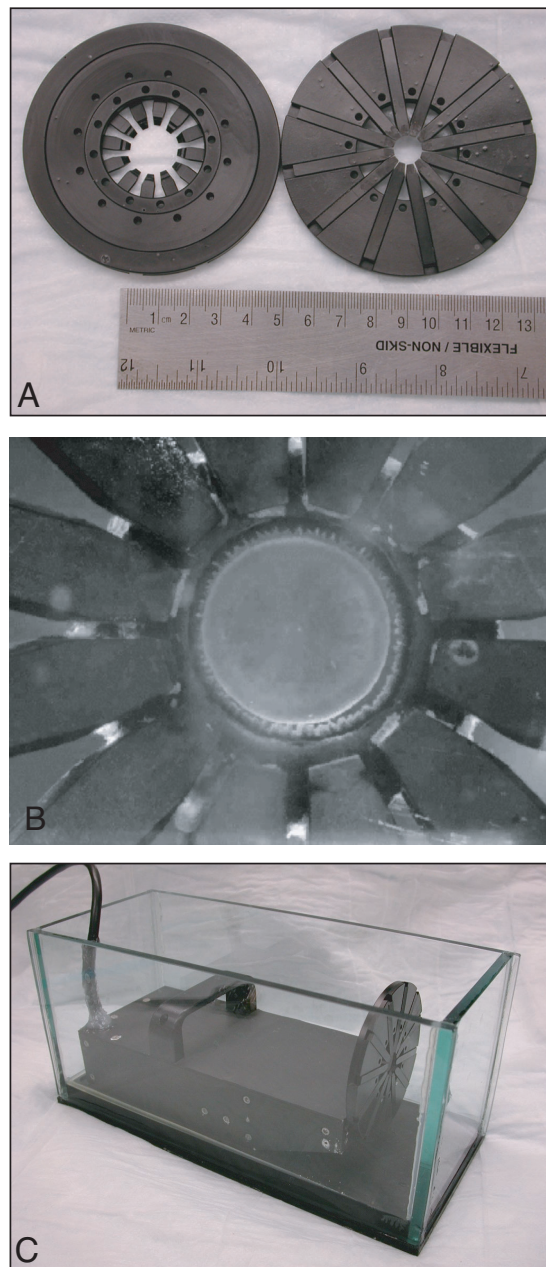


Figure 2. Mechanical stretching apparatus. (a). Front and back views of two molded plastic dilators. (b). [Lens stretching movie](#). The macaque ciliary body is glued to the arms of the dilator with the crystalline lens naturally suspended by the intact zonule. (c). Dilator mounted to the stepper motor and placed in the glass chamber. The chamber is filled with saline prior to scanning laser measurements.

rior, nasal and temporal are not tracked, they could be by placing sutures at specific locations in the ciliary body, for example.

The dilator is fixed to the front of a stepper motor mechanical stage and the entire system is placed in a rectangular glass chamber (Figure 2). The chamber is filled with saline of refractive index 1.333. A small quantity of powdered milk is added to the saline to visualize the laser beam, and the chamber is positioned so that the lens is in the path of the laser beam. The vertical position of the chamber is adjusted with a laboratory jack and the horizontal position with a manual translation stage. The chamber is carefully aligned such that the laser beam passes directly through the center of the crystalline lens suspended in the mechanical stretching apparatus. The alignment is checked by observing the two video camera images in which the entrance laser beam incident on the anterior lens surface and the exit laser beam exiting the posterior lens surface can be seen. The glass chamber is adjusted horizontally and vertically in the x and y planes to minimize the deviation of the laser beam as it passes through the lens in both the x and y planes.

The laser scanning procedure

Once the alignment procedure is completed, the x axis translation stage is moved by the computer to locate the horizontal edges of the lens. These are determined as the point at which the laser beam is just refracted as it grazes the edge of the lens. These two horizontal edges are recorded and the laser centered again. The y stage is then moved to locate the vertical edges of the lens in the same way. These positions are recorded and the laser centered again. The desired spot pattern is then calculated. This calculation considers the diameter of the lens to scan, the total number of entrance beam positions, and the beam separation. Any number and geometry of sample locations can be used and is limited only by the minimum step size of the stepper motors ($1\text{ }\mu\text{m}$) and the absolute size of the lens. In the tests described here, a grid pattern of 241 equally spaced entrance positions is used such that a circular arrangement of these spots falls within the lens diameter, constituting 17 sample positions across the lens diameter (Figure 6). Once the beam spot pattern is determined, the number of beam positions desired and the scan diameter are entered into the software macro and the scanning begins. For the analysis, three iterations are averaged to obtain one horizontal and one vertical slope and intercept value for each beam position. The number of iterations can be adjusted under software control. The sequence of moving the stages, acquiring the images, digitizing the beam paths three times with both cameras, and storing the data takes approximately 2 s. Thus the duration of the entire procedure can be calculated based on the number of beam positions and iterations chosen. The measurement of a lens with 241 beam positions and three iterations at each beam positions takes approximately 8 min.

Lens stretching

The mechanical stretching system allows the lens to be mechanically stretched via the ciliary body and intact zonular fibers (Glasser & Campbell, 1998). The ciliary body is sufficiently robust, extensible and elastic to achieve this, undamaged, without radial cuts through the tissue. This preparation relies on the lens capsule surrounding the lens to maximally accommodate the lens when the stretching tension is released. The ciliary body tissue is glued to the stretching dilator in such a way that in the unstretched state there is minimal tension on the zonular fibers. In this state, the lens is considered to be maximally accommodated. As the stretching tension is increased, the zonular fibers pull the lens equator to increase the lens diameter and effectively pull the lens into a relatively more flattened and unaccommodated state. The toothed, geared stretching apparatus under computer control is set to stretch the tissue by a specified increase in diameter of the apparatus (rather than of the tissue) in a given number of steps. The extent of stretch applied is based on the size of the tissue and the age of the animal from which it was taken. For example, a young adult rhesus monkey tissue can be reliably stretched to increase the dilator ring diameter by 3.5 mm without damage to the tissue. The smallest extent of stretch that can be applied is limited only by the stepper motor resolution ($1\text{ }\mu\text{m}$). Under software control, the system does the optical measurement as described above with the tissue in the unstretched (accommodated) state, an incremental stretch is then applied to the tissue, and the scanning laser optical measurement is repeated at each stretched state. The stretching is always done in the same direction. Once the maximum stretch is achieved, the system returns to the zero position to repeat the stretch again. This avoids any hysteresis in the stretch due to the stretching apparatus. The extent of stretch is not under feedback control, but because it is stepper motor driven, the step count determines the extent of stretch applied. Under software control, this process can be configured to automatically repeat any number of times. The optical measurements are saved to an ASCII text file together with the extent of stretch applied. After the final stretch and optical measurement, the tissue is returned to the unstretched state.

Calculation of the wave aberration

The data from the intersection points of the entrance and exit beams and the slopes of the exit beams in the horizontal and vertical planes are used to determine the mean focal length of the lens. This is the mean crossing point of each exit beam with the optical axis. The x and y deviations of each exit beam as it intersects with this mean focal plane are then computed. These x and y deviations are then used to determine the local slopes of the wavefront at each entrance beam position and then to fit the wavefront. The 3D laser-scanning technique allows the wave aberration to be derived from the slope of the wavefront, which is calculated at an array of positions across the aperture (Cubalchini,

1979). The wavefront is calculated at the entrance pupil position that roughly corresponds to the principal plane of the lens. The data analysis is no different than the Shack-Hartmann method (Liang & Williams, 1997) or other ray tracing techniques that measure wave aberrations in human eyes (He, Marcos, Webb, & Burns, 1998). In this method, the derivative of the polynomial describing the wavefront is fit to the data, using a least squares fitting method. The coefficients for the derivative of the polynomial are the same as for the original equation, so the wave aberration can be recovered directly from the fit to its derivative. The wave aberration was fit with the Zernike polynomial series, which was ordered according to the OSA standard for vision science (Thibos, Applegate, Schwiegerling, Webb, & VSIA Taskforce, 2000). Analysis was done with custom software written in Visual C++. The analysis program allows for any number of sample locations and can fit any number of Zernike terms. Many image quality metrics can be calculated once a mathematical representation of the wave aberration has been fit. All metrics shown are derived from the wave aberration.

Results

Testing and verification

The technique was tested by measuring the wave aberration of a 25-mm focal length standard plano-convex lens (Newport Corp.) that was immersed in water. The lens was scanned three times in succession, by removing the lens from the chamber and replacing it again each time. Slopes of the wavefront were measured in the x and y directions at 241 points in an evenly spaced grid pattern that filled the circular aperture of the lens. The wave aberration, analyzed over 19 mm was fit to a 7th order Zernike polynomial. ZEMAX optical design software (Focus Software Inc.) was used to calculate the wave aberrations of the same glass lens based on its catalog description using the same parameters as defined in the scanning laser software. Figure 3 shows a bar graph comparing the Zernike terms (with SDs from the three measurements) obtained from both techniques. Optical modeling showed that only rotationally symmetric aberrations are present in the lens, mainly 4th and 6th order spherical aberration. The experimental results are similar, but also show some additional coma and astigmatism. The presence of these additional aberrations can easily arise with a small amount of decentration of the sampling pattern along with tilt of the lens in the apparatus.

Porcine crystalline lens

As a first test of a crystalline lens, the wave aberration of a porcine lens was measured. The lens was dissected from the eye and mounted in the lens chamber with the anterior lens surface facing forward and the wave aberrations measured over an entrance pupil diameter of 7 mm. Figure 4 shows a plot of the Zernike terms fit up to the 7th

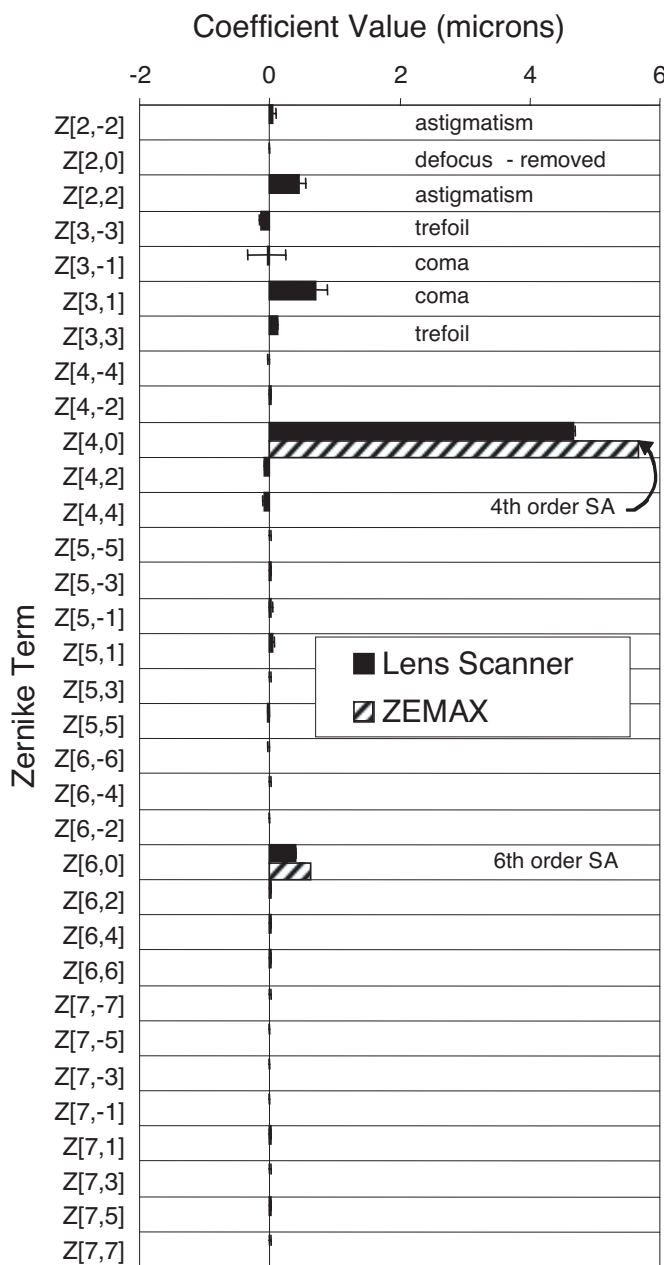


Figure 3. Zernike polynomial coefficient values for experimental and ZEMAX calculations of a 25-mm diameter plano-spherical lens analyzed with a 19-mm diameter in both cases. Error bars represent SDs for three separate measurements of the glass lens.

order. This crystalline lens has a myriad of low- and high-order aberrations. In addition to negative spherical aberration, the next most dominant aberrations are trefoil and a secondary trefoil Z_5^{-3} , both of which have threefold symmetry. These threefold symmetric terms account for the three lobes that are readily visible in the contour plots of the calculated wave aberration (Figure 5).

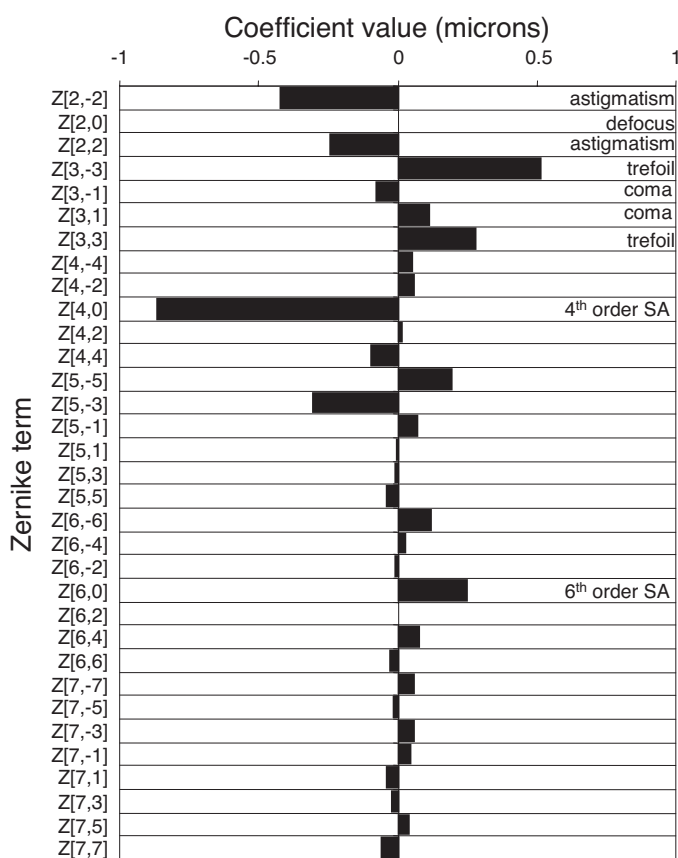


Figure 4. Zernike polynomial coefficient values for an isolated porcine lens.

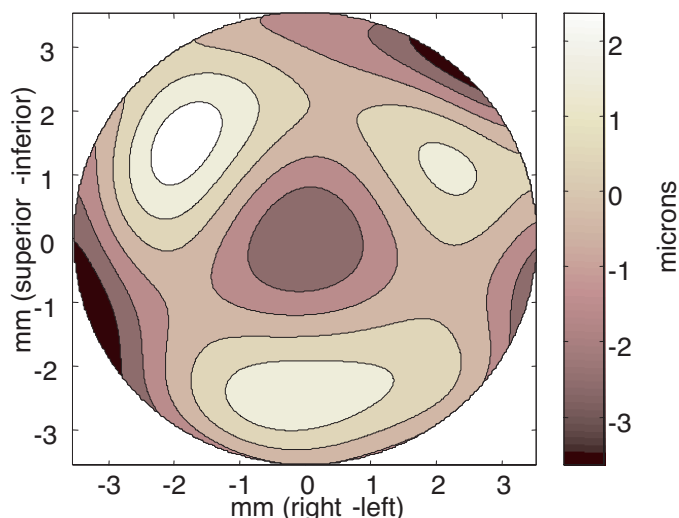


Figure 5. Contour plot of the wave aberration of an isolated porcine lens.

Accommodating macaque lens

To determine lenticular aberration changes with accommodation, the wave aberration of an isolated crystalline lens from a macaque monkey was measured as a function of changing power induced by mechanical stretching. In these experiments, the sampling grid was initially set to sample the full aperture of the unstretched lens, which was just under 7 mm in diameter. As the lens was stretched, the sample positions remained fixed. Thus, the effective entrance pupil size remained the same, but the sampling pattern covered a smaller fraction of the lens surface. Figure 6 shows the 241-point sampling grid superimposed on the lens in the unstretched state.

The wave aberrations were computed over a 6-mm entrance pupil for 6 stretch states, ranging from fully stretched to fully relaxed. Table 1 shows the focal length, focal power, and root mean square (RMS) aberration, (calculated for all

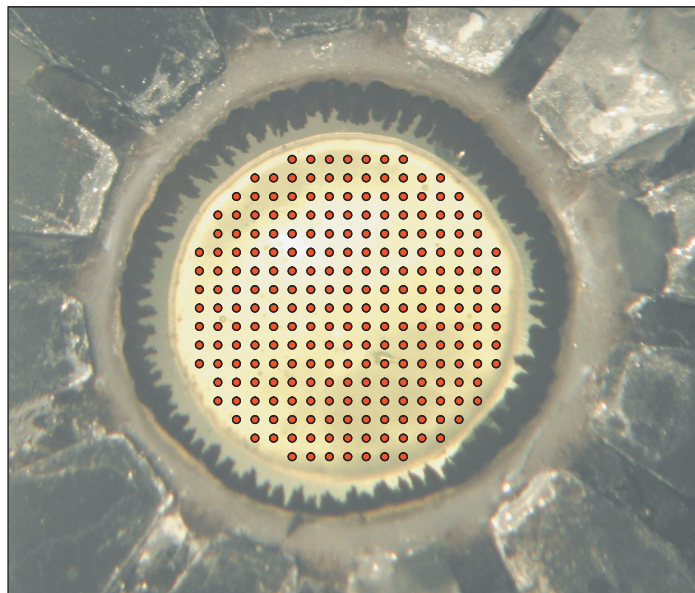


Figure 6. Sampling geometry superimposed on the mounted macaque lens. The sampling grid comprises 241 points in a grid over a circular pupil. The spacing between samples on the grid is 0.4 mm.

Stretch amount (mm)	Focal length (mm)	Focal power (D)	RMS aberration (microns)
0	25.8	38.8	3.35
0.58	30.1	33.3	2.99
1.17	37.0	27.1	2.18
1.75	40.2	24.9	2.00
2.33	42.0	23.8	2.08
2.92	43.9	22.8	2.15

Table 1. Focal length and focal power were calculated as the image plane that minimized the root mean square (RMS) aberration. The stretch amount refers to the change in diameter of the arms of the stretching apparatus, not to the change in diameter of the lens itself.

terms except defocus) for each stretch position. The focal plane that minimized the RMS aberration was used to select the focal power of the lens at each stretch state. Figure 7 shows contour plots of the wave aberrations of the macaque lens for the six increasing stretched states. Figure 8 shows a bar graph of the wave aberrations of all terms excluding defocus for each stretch state. Defocus is not shown because the magnitude of its change was much larger than any other aberration. This plot reveals a systematic change in aberration structure of most terms with stretching. The most dominant changes occur for 4th and 6th order spherical aberration. For the 4th order spherical aberration, the aberration starts negative and becomes more negative as the power of the lens increases (as stretching decreases). The reverse happens for 6th order spherical aberration where the coefficient starts negative and progresses to a positive value with accommodation.

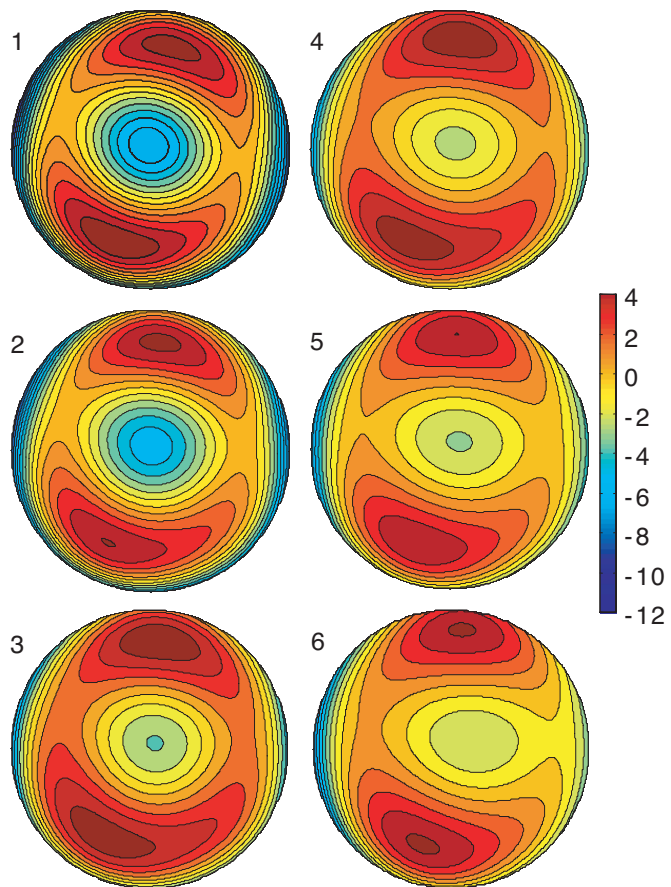


Figure 7. Contour plots of the wave aberrations of the macaque lens as it is disaccommodated (by stretching the ciliary body). The defocus term is not included in these contour plots. Contour plot 1 represents the wave aberrations in the unstretched (accommodated) state. The scale is in microns.

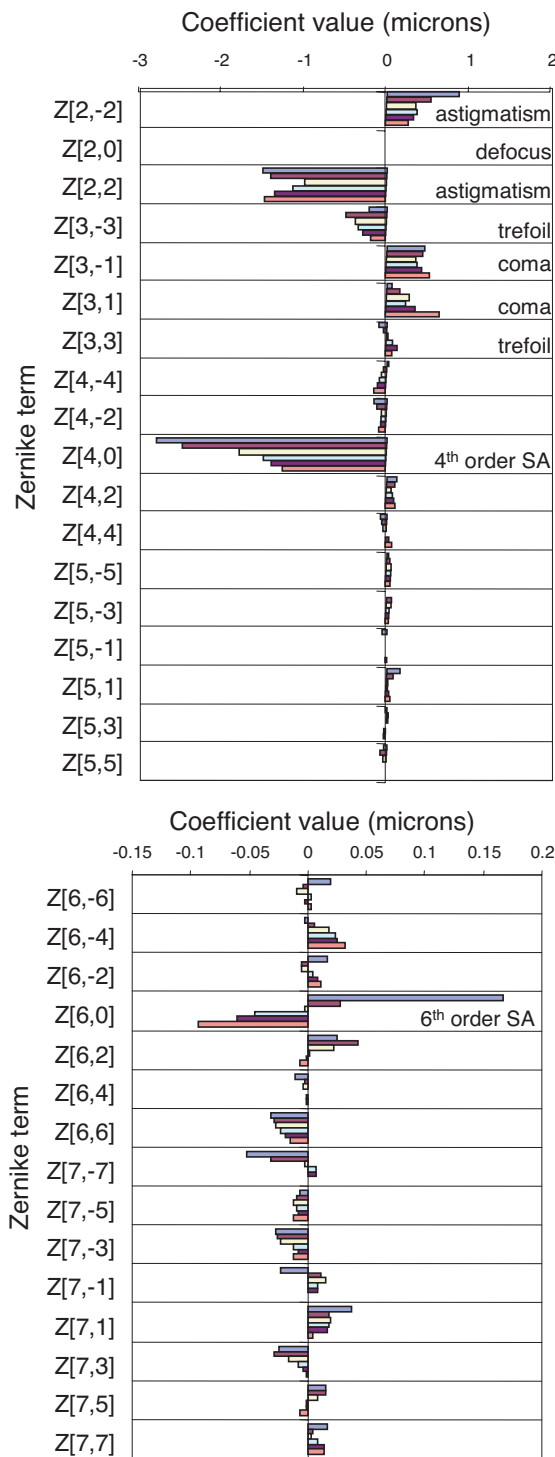


Figure 8. Zernike polynomial coefficient values for the macaque lens. Six bars are shown for each Zernike term, representing the coefficient value for each stretch state. For each term, the stretch is increasing from top to bottom; therefore, accommodation increases from bottom to top. The 4th order spherical aberration becomes more negative with accommodation, whereas 6th order spherical aberration becomes more positive. Two plots are shown to represent all the terms considered with different scales due to the differences in the magnitudes of the aberrations.

Discussion

Validity of this approach

This SLOPE method offers several important benefits, but also some drawbacks. Any number of beams can be positioned on the lens, high aberrations can be measured by virtue of the sequential analysis of each beam, lenses of considerably varying sizes can be measured, all with the same spot pattern and same number of beams, within the software/hardware constraints of the system. In contrast, a Shack-Hartmann system relies on the lenslet array to define the spot pattern. In addition, physiological lenses can readily be measured in a saline environment that is necessary to ensure optimal quality of the lens. A 6-mW laser provides a robust beam that allows lenses of imperfect optical quality to be measured because the exit beam is still readily visible in the solution.

Limitations of this approach include that it is slower than a Shack-Hartman system that captures a single image to do the entire analysis. Alignment of a physiological lens in an optomechanical system presents some unique challenges. Isolated physiological lenses, such as pig lenses, are variable in shape and size, they have no well defined shape, edges or optical axis and can easily be damaged. This makes it difficult, perhaps impossible, to align a physiological lens in an optical instrument with any degree of certainty. But the same drawbacks would arise for any method used to measure physiological lenses. Future efforts will be directed at exploring mounting and alignment tools to reduce this source of variability.

There are some differences between the measured aberrations of the glass lens and the idealized calculations. These differences could stem from misalignment of the glass lens in the optical system. Because the system is designed to measure physiological lenses, the glass lens was aligned in the same way the physiological lenses were aligned. No special provision has been made for critical optical alignment of a glass lens. The error bars, representing the *SD* of three separate measurements, show that the measurements are consistent. While the measured values show the existence of coma and astigmatism, most likely resulting from tilt of the glass lens, there is also a 1-micron difference in the extent of the spherical aberration. This could be due to slight differences between the actual scan diameter and the calculated scan diameter. In the glass lens, which had a high degree of spherical aberration, ZEMAX modeling demonstrated that only a 3.5% difference (0.65 mm) in the analyzed entrance pupil diameter could account for the difference between the calculated and the measured values. The same change in scan diameter for a 10-mm aperture in the same lens caused in a difference in the spherical aberration coefficient of only 0.07 microns. It is impossible to get a good idea of the variability in this method from the results of different physiological lenses. Lenses exhibit considerable variability, so comparisons between

different lenses offer little information on variability of the method versus variability of the lenses. The relatively consistent and systematic changes that resulted with the repeated measurements of the monkey lens suggest that the method is reliable. Additional testing underway will consider other approaches to understand the repeatability and reliability of the method.

Measurement of lens aberrations

The goal of this study was to measure the aberrations of the entire lens to begin to understand the aberration structure of the lens alone and how it may change with aging and accommodation. The approach considers only parallel rays entering the isolated lens. This would produce an aberration structure fundamentally different to the lens inside an eye that has convergent rays impinging on it due to refraction by the cornea. *In vivo*, the iris covers most of the lens, thus reducing the entrance pupil diameter considerably for vision. In this study, the aberrations were measured over the full lens diameter. Certainly, the aberrations of the lens will be considerably lower for smaller analyzed entrance pupil diameters. However, because no information is available about the aberrations due to the cornea in these pig and monkey eyes, it is not particularly relevant to consider the aberrations over smaller diameters in an effort to understand the implications of the lens aberrations to vision in these eyes. It would be of relevance to compare the extent of the aberrations of the pig and monkey lenses with those of the human lens. However, to our knowledge, no wave aberrations have been made of the human lens alone. Aberrations due to the cornea subtracted from the aberrations due to the entire eye do provide some information on the lens aberrations (Artal et al., 2002; Artal & Guijarro, 1998). However, this is an indirect approach, which is subject to errors due to ignoring the aberrations of the posterior corneal surface and due to converging rays impinging on the lens. Because this approach also considers only the aberrations of the eye as measured through the pupillary aperture, this again does not offer a very satisfying comparison to the aberrations measured over the full lens diameter in this study.

Spherical aberration

Unlike a typical biconvex positive lens, the bovine and macaque crystalline lens decrease in power toward the periphery, or exhibit negative spherical aberration. Negative spherical aberration is found in the crystalline lens of many species [pig (Vilupuru & Glasser, 2001); young human (Glasser & Campbell, 1998); rat (Campbell & Hughes, 1981); fish (Kröger et al., 1994); and chicken (Glasser & Howland, 1995)]. Crystalline lenses have negative spherical aberrations because of a gradient index of refraction, which peaks at the core and reduces toward the cortex (Campbell & Hughes, 1981). By comparison, uniform refractive index crystalline lens models that are defined only by surface curvatures suffer from a great deal of positive spherical aberra-

tion (Campbell & Hughes, 1981). The negative spherical aberration of the crystalline lens is thought to play a role in reducing the aberrations of the whole eye by compensating for the positive spherical aberration that is found in the typical cornea (Artal et al., 2001).

Nonsymmetric aberrations

To our knowledge, this study represents the first study to measure the wave aberrations of isolated lenses. In addition to rotationally symmetric aberrations, nonsymmetric aberrations were also observed in both kinds of lenses. Some of the aberrations were due possibly to misalignments and decentration of the scanning system and small tilts in the lens. Such errors were also apparent in the measurements of the glass lens, which is not expected to have any asymmetric aberrations. Although alignment was controlled as much as possible, high power, bi-convex optics degrade quickly with tilt and decentration. Nonsymmetric aberrations in the macaque lens preparation might also be due to nonuniform tension in the stretching apparatus. It is likely, however, that physiological lenses do exhibit nonsymmetrical aberrations and that these aberrations are not all artifacts. For example, the predominant threefold symmetry observed in the porcine lens cannot be induced by a tilt or decentration. Such nonsymmetric aberrations have been reported previously in porcine lenses (Vilupuru & Glasser, 2001). Observations of the shape and structure of the pig lenses make it clear that these lenses are not idealized symmetrical lenses. The wave aberration measurements reported here provide more detailed information on these aberrations than was previously available from measurements in one meridian only (Vilupuru & Glasser, 2001). This three-fold wave aberration shape might be the result of optical aberrations due to the "Y" suture patterns in the porcine lens (Kuszak, Peterson, Sivak, & Herbert, 1994).

Changes with accommodation

The mechanical stretching is designed to simulate rather than reproduce accommodation exactly. There are several important differences. The vitreous and the intraocular pressure is absent; the direction of the forces involved with stretching is not identical to those that occur in vivo with accommodation. However, prior studies have shown that the results from mechanical stretching experiments provide good correspondence between in vivo and in vitro results in terms of the optical changes in the lens (Glasser & Campbell, 1998).

Large systematic aberration changes in the macaque lens were observed with mechanical stretching designed to produce accommodative changes in the lens. The predominant change was in the 4th order spherical aberration, which became less negative with stretching. The same result was seen in previous studies of human lenses (Glasser & Campbell, 1998) and is also observed in vivo during accommodation in iridectomized rhesus monkey eyes (Vilu-

puru, Roorda, & Glasser, 2004). In the present study, RMS of all aberrations (excluding defocus) increased as the lens became more accommodated. In the intact human eye, it has been reported that ocular aberrations reduce with accommodation to a point and then increase again (He & Marcos, 2000). These two effects are compatible for the following reason: In the unaccommodated state, the whole eye aberrations are dominated by the positive spherical aberrations of the cornea. With accommodation, the increasing negative spherical aberration of the lens compensates for the cornea until, at some point, the compensation is optimal and the whole eye RMS aberration is at a minimum. Further increases of the negative spherical aberration of the lens from accommodation over-compensate for the cornea and increases the whole eye aberration again.

Caution should be exhibited in extrapolating these in vivo results of the accommodation aberration changes in the isolated lens to in vivo results of how ocular aberrations change with accommodation in the eye (Hofer et al., 2001). The intact eye is composed of the two optical elements, the cornea and the lens. Accommodative induced lens tilt, sag, or decentration can have an impact on the aberrations of the whole eye, such as introducing astigmatism and coma, for example. The in vivo results are not subject to this because it is just the single optical element, the lens, that is under consideration. The results shown here for the rhesus monkey lens show relatively small changes in coma and astigmatism relative to the more pronounced changes in spherical aberrations, for example. This is suggestive that the mechanical stretching system is producing a symmetric change to the lens and that the lens changes are relatively symmetrical.

This tissue preparation relies on the lens capsule molding the lens into an accommodated form when lens equatorial zonular tension is at a minimum. In primates, accommodation occurs due to a release in zonular tension at the lens equator (Helmholtz, 1909; Glasser & Kaufman, 1999). The prevailing view is that the lens becomes more spherical with accommodation due to the molding force of the capsule (Fincham, 1937). This would be expected to result in lens spherical aberration becoming more positive with accommodation (i.e., peripheral power increasing more than paraxial power). However, the results actually demonstrate that accommodation of the lens is accompanied by an increase in negative spherical aberration. A similar result was observed with mechanical stretching of human lenses (Glasser & Campbell, 1998) and is observed in vivo with accommodation in iridectomized rhesus monkey eyes (Vilupuru, Roorda, & Glasser, 2004).

The increasing negative spherical aberration of the accommodating lens arises from a more pronounced increase in optical power near the central region of the lens compared to the peripheral region. In other words, as the lens accommodates, the central curvature steepens while the peripheral curvature flattens. This is different to the generally accepted notion that the lens simply becomes more spherical with accommodation. The increase in negative

spherical aberration is likely due to the effect of the structure of the lens substance and varying surface thickness and elasticity of the capsule acting to increase the curvature near the center of the lens more than at the periphery (Fincham, 1937) but may also in part be due to accommodative variations in gradient refractive index of the lens. It is well established that the lens undergoes changes in surface curvature with accommodation, but accommodative changes in lens refractive index gradient are less certain, thus suggesting that is more likely that the changes in spherical aberration are due to changes in lens surface curvature. Because lens accommodative changes can be well described by changes in surface curvature, if both lens curvature and refractive index change with accommodation, it is likely that the changes in curvature would dominate the changes in the gradient.

A catenary suspension theory of accommodation could potentially explain this accommodative shape of the lens (Coleman, 1986; Coleman & Fish, 2001; Coleman, 2002). However, in this dissected, reduced tissue preparation, the catenary due to the vitreous is not present and the capsule is the only force available to accommodate the lens. This data together with prior experiments on accommodation in isolated human lenses support the Helmholtz theory and capsular basis of accommodation (Helmholtz, 1909; Fincham, 1937)

Conclusions

Wave aberrations have been measured from isolated crystalline lenses with a laser ray-tracing technique as a function of mechanically induced accommodative changes in the lens. This new method of measuring wave aberrations over the lens surface rather than a single meridian provides valuable insights into the optical and accommodative performance of the crystalline lens and increases the utility of in vitro lens studies.

Acknowledgments

The authors thank Lingyun Hu for writing the SLOPE software, Hope Queener and Chris Kuether for technical assistance, and Yuzo Chino for providing macaque lenses. This study was funded in part by a grant from Pharmacia to AR and AG and National Institutes of Health Grant RO1 EY 014651-01 to AG.

Commercial relationships: none.

Corresponding author: Austin Roorda.

Email: aroorda@uh.edu.

Address: University of Houston College of Optometry, Houston, TX, USA.

References

- Artal, P., Berrio, E., Guirao, A., & Piers, P. (2002). Contribution of the cornea and internal surfaces to the change of ocular aberrations with age. *Journal of the Optical Society of America A*, 19, 137-143. [PubMed]
- Artal, P., & Guirao, A. (1998). Contribution of the cornea and lens to the aberrations of the human eye. *Optics Letters*, 23, 1713-1715.
- Artal, P., Guirao, A., Berrio, E., & Williams, D. R. (2001). Compensation of corneal aberrations by the internal optics in the human eye. *Journal of Vision*, 1(1), 1-8, <http://journalofvision.org/1/1/1>, doi:10.1167/1.1.1. [PubMed] [Article]
- Atchison, D. A., Collins, M. J., Wildsoet, C. F., Christensen, J., & Waterworth, M. D. (1995). Measurement of monochromatic ocular aberrations of human eyes as a function of accommodation by the Howland aberrometer technique. *Vision Research*, 35, 313-323. [PubMed]
- Axelrod, D., Lerner, D., & Sands, P. J. (1988). Refractive index within the lens of a goldfish eye determined from the paths of thin laser beams. *Vision Research*, 28, 57-65. [PubMed]
- Barbero, S., Marcos, S., & Merayo-Lloves, J. (2002). Corneal and total optical aberrations in a unilateral aphakic patient. *Journal of Cataract Refractive Surgery*, 28, 1594-1600. [PubMed]
- Campbell, M. C. W. (1984). Measurement of refractive index in an intact crystalline lens. *Vision Research*, 24, 409-415. [PubMed]
- Campbell, M.C.W., & Hughes, A. (1981). An analytic gradient index schematic lens and eye for the rat which predicts aberrations for finite pupils. *Vision Research*, 21, 1129-1148. [PubMed]
- Chan, D. Y. C., Ennis, J. P., Pierscionek, B. K., & Smith, G. (1988). Determination and modeling of the 3-D gradient refractive indices in crystalline lenses. *Applied Optics*, 27, 926-931.
- Cheng, H., Barnett, J. K., Vilupuru, A. S., Marsack, J. D., Kasthurirangan, S., Applegate, R. A., & Roorda, A. (2004). A population study on changes in wave aberration with accommodation. *Journal of Vision*, 4 (4), 272-280, <http://journalofvision.org/4/4/3/>, doi:10.1167/4.4.3. [PubMed] [Article]
- Coleman, D. J. (1986). On the hydraulic suspension theory of accommodation. *Transactions of the American Ophthalmological Society*, 84, 846-868. [PubMed]
- Coleman, D. J. (2002). Presbyopia, accommodation, and mature catenary: Author reply. *Ophthalmology*, 109, 1416-1418.

- Coleman, D. J., & Fish, S. K. (2001). Presbyopia, accommodation, and the mature catenary. *Ophthalmology*, 108, 1544-1551. [\[PubMed\]](#)
- Cubalchini, R. (1979). Modal wave-front estimation from phase derivative measurements. *Journal of the Optical Society of America*, 69, 972-977.
- Dovrat, A., Sivak, J. G., & Gershon, D. (1986). Novel approach to monitoring lens function during organ culture. *Lens Research*, 3, 207-215.
- Fincham, E. F. (1937). The mechanism of accommodation. *British Journal of Ophthalmology, Monograph VIII*, 7-80.
- Glasser, A., & Campbell, M. C. W. (1998). Presbyopia and the optical changes in the human crystalline lens with age. *Vision Research*, 38, 209-229. [\[PubMed\]](#)
- Glasser, A., & Campbell, M. C. W. (1999). Biometric, optical and physical changes in the isolated human crystalline lens with age in relation to presbyopia. *Vision Research*, 39, 1991-2015. [\[PubMed\]](#)
- Glasser, A., & Howland, H. C. (1995). In vitro changes in back vertex distance of chick and pigeon lenses: Species differences and the effects of aging. *Vision Research*, 35, 1813-1824. [\[PubMed\]](#)
- Glasser, A., & Kaufman, P. L. (1999). The mechanism of accommodation in primates. *Ophthalmology*, 106, 863-872. [\[PubMed\]](#)
- Guirao, A., & Artal, P. (2000). Corneal wave aberration from videokeratography: Accuracy and limitations of the procedure. *Journal of the Optical Society of America A*, 17, 955-965. [\[PubMed\]](#)
- He, J. C., Burns, S. A., & Marcos, S. (2000). Monochromatic aberrations in the accommodated human eye. *Vision Research*, 40, 41-48. [\[PubMed\]](#)
- He, J. C., Marcos, S., Webb, R. H., & Burns, S. A. (1998). Measurement of the wavefront aberration of the eye by a fast psychophysical procedure. *Journal of the Optical Society of America A*, 15, 2449-2457. [\[PubMed\]](#)
- Helmholtz, H. (1909). Mechanism of accommodation. In J. P. C. Southall (Ed.), *Helmholtz's treatise on physiological optics* (pp. 143-173). New York: Dover.
- Hofer, H., Artal, P., Aragon, J. L., & Williams, D. R. (2001). Dynamics of the eye's wave aberration. *Journal of the Optical Society of America A*, 18, 497-506. [\[PubMed\]](#)
- Ivanoff, A. (1956). About the spherical aberration of the eye. *Journal of the Optical Society of America*, 46, 901-903.
- Jenkins, T. C. A. (1963). Aberrations of the eye and their effects on vision: Part I. *British Journal of Physiological Optics*, 20, 59-91.
- Koomen, M., Tousey, R., & Scolnik, R. (1949). The spherical aberration of the human eye. *Journal of the American Optometric Association*, 39, 370-376.
- Kröger, R. H. H., Campbell, M. C. W., & Fernald, R. D. (2001). The development of the crystalline lens is sensitive to visual input in the African cichlid fish, *Haplochromis burtoni*. *Vision Research*, 41, 549-559. [\[PubMed\]](#)
- Kröger, R. H. H., Campbell, M. C. W., Munger, R., & Fernald, R. D. (1994). Refractive index distribution and spherical aberration in the crystalline lens of the African cichlid fish *haplochromis burtoni*. *Vision Research*, 34, 1815-1822. [\[PubMed\]](#)
- Kreuzer, R. O., & Sivak, J. G. (1985). Chromatic aberration of the vertebrate lens. *Ophthalmic and Physiological Optics*, 5, 33-41. [\[PubMed\]](#)
- Kuszak, J. R., Peterson, K. L., Sivak, J. G., & Herbert, K. L. (1994). The interrelationship of lens anatomy and optical quality II: Primate lenses. *Experimental Eye Research*, 59, 521-535. [\[PubMed\]](#)
- Liang, J., & Williams, D. R. (1997). Aberrations and retinal image quality of the normal human eye. *Journal of the Optical Society of America A*, 14, 2873-2883. [\[PubMed\]](#)
- Lu, C., Campbell, M. C. W., & Munger, R. (1994). Monochromatic aberrations in accommodated eyes. *Ophthalmic and Visual Optics Technical Digest* (OSA, Washington, D.C.), 3, 160-163.
- Marcos, S. (2001). Aberrations and vision performance following standard laser vision correction. *Journal of Refractive Surgery*, 17, S596-S601. [\[PubMed\]](#)
- Millodot, M., & Sivak, J. (1979). Contribution of the cornea and lens to the spherical aberration of the eye. *Vision Research*, 19, 685-687. [\[PubMed\]](#)
- Pierscionek, B. K., Chan, D. Y. C., Ennis, J. P., Smith, G., & Augusteyn, R. C. (1988). Nondestructive method of constructing three-dimensional gradient index models for crystalline lenses: I. Theory and experiment. *American Journal of Optometry and Physiological Optics*, 65, 481-491. [\[PubMed\]](#)
- Salmon, T. O., and Thibos, L. N. (2002). Videokeratoscope line of sight misalignment and its effect on measurements of corneal and internal ocular aberrations. *Journal of the Optical Society of America A*, 19, 657-669. [\[PubMed\]](#)
- Sivak, J. G. (1982). The contribution of the crystalline lens to chromatic and spherical aberrations of the eye. *Canadian Journal of Optometry*, 44, 89-91.
- Sivak, J. G., & Dovrat, A. (1983). Aging and the optical quality of the rat crystalline lens. *Investigative Ophthalmology and Visual Science*, 24, 1162-1166. [\[PubMed\]](#)
- Sivak, J. G., & Kreuzer, R. O. (1983). Spherical aberration of the crystalline lens. *Vision Research*, 23, 59-70. [\[PubMed\]](#)

- Thibos, L. N., Applegate, R. A., Schwiegerling, J., Webb, R. H., & VSIA Standards Taskforce Members (2002). Standards for reporting the optical aberrations of eyes. *Journal of Refractive Surgery*, 18, S652-S660. [PubMed]
- Vilupuru, A. S., & Glasser, A. (2001). Optical and biometric relationships of the isolated pig crystalline lens. *Ophthalmic and Physiological Optics*, 21, 296-311. [PubMed]
- Vilupuru, A. S., Roorda, A., & Glasser, A. (2004). Spatially variant changes in lens power during ocular accommodation in a rhesus monkey eye. *Journal of Vision*, 4(4), 299-309, <http://journalofvision.org/4/4/6/>, doi: 10.1167/4.4.6. [PubMed] [Article]
- Williams, D. R., Yoon, G., Guirao, A., Hofer, H., & Porter, J. (2001). How far can we extend the limits of human vision? In S. M. Macrae, R. R. Krueger, & R. A. Applegate (Eds.), *Customized corneal ablation: The quest for supervision* (pp. 11-32). Thorofare, NJ: Slack, Incorporated.